K^+-Translocating KdpFABC P-Type ATPase from *Escherichia coli* Acts as a Functional and Structural Dimer†

Thomas Heitkamp,‡ René Kalinowski,§ Bettina Böttcher,|| Michael Börsch,⊥ Karlheinz Altendorf,‡ and Jörg-Christian Greie*,‡

Universität Osnabrück, Fachbereich Biologie/Chemie, Arbeitsgruppe Mikrobiologie, 49069 Osnabrück, Germany, Scriptor Dokumentations Service GmbH, Krackser Strasse 12C, 33659 Bielefeld, Germany, EMBL Heidelberg, Meyerhofstrasse 1, 69117 Heidelberg, Germany, and Physikalisches Institut, Pfaffenwaldring 57, 70550 Stuttgart, Germany

Received October 11, 2007; Revised Manuscript Received January 11, 2008

ABSTRACT: The membrane-embedded K^+-translocating KdpFABC complex from *Escherichia coli* belongs to the superfamily of P-type ATPases, which share common structural features as well as a well-studied catalytic mechanism. However, little is known about the oligomeric state of this class of enzymes. For many P-type ATPases, such as the Na^+/K^+-ATPase, Ca^{2+}-ATPase, or H^+-ATPase, an oligomeric state has been shown or is at least discussed but has not yet been characterized in detail. In the KdpFABC complex, kinetic analyses already indicated the presence of two cooperative ATP-binding sides within the functional enzyme and, thus, also point in the direction of a functional oligomer. However, the nature of this oligomeric state has not yet been fully elucidated. In the present work, a close vicinity of two KdpB subunits within the functional KdpFABC complex could be demonstrated by chemical cross-linking of native cysteine residues using copper 1,10-phenanthroline. The cysteines responsible for cross-link formation were identified by mutagenesis. Cross-linked and non-cross-linked KdpFABC complexes eluted with the same apparent molecular weight during gel filtration, which corresponded to the molecular weight of a homodimer, thereby clearly indicating that the KdpFABC complex was purified as a dimer. Isolated KdpFABC complexes were analyzed by transmission electron microscopy and exhibited an approximately 1:1 distribution of mono- and dimeric particles. Finally, reconstituted functional KdpFABC complexes were site-directedly labeled with flourescent dyes, and intermolecular single-molecule FRET analysis was carried out, from which a dissociation constant for a monomer/dimer equilibrium between 30 and 50 nM could be derived.

In all kingdoms of life, P-type ATPases are involved in transporting cations across biological membranes at the expense of ATP (*1*). These ions play crucial roles in living cells as, for example, enzyme cofactors and cosubstrates for sym- and antiport processes, and they are involved in the maintenance of cytoplasmic pH and turgor. Most of the knowledge about P-type ATPases was obtained from detailed studies of eukaryotic P-type ATPase, especially from the elucidation of the structure of the sarco(endo)plasmic reticulum Ca^{2+}-ATPase (SERCA) at various stages of the reaction cycle (*2*–*6*).

Characteristic for the reaction cycle of P-type ATPases is the presence of two major conformational as well as catalytic states named E1 and E2. Large domain movements between these states, which are mainly triggered by the formation of a transient phospho-intermediate at a conserved Asp residue, result in different binding affinities for both ATP and the transport substrate (*1*).

Whereas the closely related eukaryotic P-type ATPases predominantly consist of only one subunit, which mediates both ATP hydrolysis and ion transport, the KdpFABC complex, which can be found in bacteria and archea, represents a rather unusual member of the P-type ATPase family. The KdpFABC complex of *Escherichia coli* is an inducible, high-affinity potassium uptake system, the synthesis of which is highly induced when the other K^+-scavenging systems are unable to meet the need of the cells for potassium. An absolutely unique feature of this P-type ATPase is the division of labor between the subunits. The KdpB subunit (72 kDa) shares homologies to other P-type ATPases and represents the catalytical subunit performing ATP hydrolysis, whereas KdpA (59 kDa) shows similarities to KcsA-like K^+-channel proteins and is known to be the ion-translocating subunit (*7, 8*). For the coupling between ATP hydrolysis and ion transport, two conserved charged residues within a transmembrane helix of KpdB were shown to be essential (*9*). KdpF (3 kDa) consists of only one hydrophobic transmembrane domain and is supposed to stabilize the complex (*10*). The 20 kDa KdpC subunit also contains just one N-terminal transmembrane span, with the

† This work was supported by the Deutsche Forschungsgemeinschaft (SFB431), the Fonds der Chemischen Industrie, and the Ministerium für Wissenschaft and Kultur of the State of Lower Saxony.

* To whom correspondence should be addressed: Universität Osnabrück, Fachbereich Biologie/Chemie, Barbarastrasse 11, 49076 Osnabrück, Germany. Telephone: +49-541-9692809. Fax: +49-541-9692870. E-mail: greie@biologie.uni-osnabrueck.de.

‡ Universität Osnabrück.

§ Scriptor Dokumentations Service GmbH.

|| EMBL Heidelberg.

⊥ Physikalisches Institut.

10.1021/bi702038e CCC: $40.75
Published on Web 02/26/2008

rest of the polypeptide facing the cytoplasm (*11*). The soluble portion of KdpC has recently been shown to bind ATP and to potentially act as a catalytic chaperone in the nucleotide-binding mechanism (*12*).

Whereas detailed information on P-type ATPases is available for isolated subunits as well as for their mode of action, comparatively little is known about their physiological and functional oligomeric state. For many P-type ATPases, a di- or multimeric structure has been shown or discussed. The H^+-ATPase from *Neurospora crassa* was demonstrated to form an active ring-like hexamer, although monomers were found to be active (*13, 14*). Detailed studies on the oligomeric form of the Na^+/K^+-ATPase led to the suggestion that the functional state of the enzyme in the membrane is a tetramer (*15*). A possible dimeric structure for SERCA has been discussed because of cross-linking studies and radiation inactivation experiments (*16–19*). For the KdpFABC complex, kinetic analysis supports the presence of two cooperative ATP-binding sites during catalysis, thus rendering the formation of a functional homodimer likely.

In this study, the oligomeric state of isolated as well as functionally reconstituted KdpFABC complexes were investigated in detail with a combination of site-directed chemical cross-linking, size-exclusion chromatography, electron microscopic analyses, and single-molecule fluorescence detection of dimers by fluorescence resonance energy transfer (FRET)[1] measurements. The results obtained revealed that also the KdpFABC complex exhibits a dimeric state above concentrations of 30–50 nM, whereas at lower concentrations, the complex exists as a functional monomer.

EXPERIMENTAL PROCEDURES

Bacterial Strains and Growth Conditions. For the expression of *kdpFABC* wild type and mutants, strain TKW3205 (Δ*kdpABC'05 nagA- trkA405 trkD1 Datp706*) was used, which contains no functional K^+ uptake system but still carries the chromosomal *kdpDE* operon for K^+-induced *kdpFABC* expression. This strain was transformed with one of the plasmids listed below. All plasmids are derivatives of plasmid pGS4 carrying the *kdpFABC* genes under control of the *kdp* promotor. In addition, the *kdpA* gene comprises a 3′ $(CATCAC)_7$ extension coding for a C-terminal His_{14} tag. TKW3205 cells transformed with pGS4 derivatives were grown in K0 medium and were induced twice with 45 μM KCl for protein synthesis according to ref *20*.

Generation of kdpB Mutants. For the cross-link analyses of native cysteines in KdpB, KdpB-C48A and KdpB-C679A exchanges were generated in the *kdpB* gene by use of the two-step PCR technique with pGS4 as the template. The C48A-coding PCR fragment was subsequently cloned into pGS4 via *Mfe* I and *Hpa* I restriction sites, and the C679A-coding fragment was cloned by *Bam*H I and *Eco*R I. For the site-specific incorporation of fluorescent FRET labels, all native cysteines in the KdpFABC complex, except residues C261 and C609 of KdpB, were replaced by alanine or serine by use of a two-step PCR technique (primer list available from the author upon request). The resulting plasmid pGS4ΔCys-KdpB(C261/C609) was used for the site-directed introduction of a cysteine residue at the position of the exposed alanine 150 in the A domain of KdpB with a two-step PCR technique (Figure 1). The corresponding PCR product was cloned into pGS4ΔCys-KdpB(261C/609C) via the restriction sites *Mfe* I and *Hpa* I, resulting in plasmid pGS4ΔCys-KdpB(C261/C609/G150C).

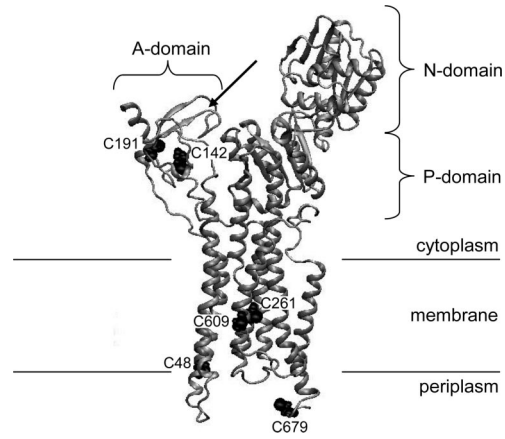

FIGURE 1: SERCA-derived (SERCA coordinates 1SU4) homology modeling of the KdpB subunit. Backbone modeling was performed by use of combined one- and three-dimensional sequence similarity patterns with PsiPred2. Occasionally occurring one- or two-residue structural gaps within the PsiPred2-derived model as a consequence of gaps within the structural sequence similarity alignment were closed manually by use of Swiss-PdbViewer V3.70b. For the N domain, the NMR-derived KdpBN coordinates 2A29 were incorporated in the model. Finally, the model was checked for possible sterical clashes and refined with respect to side-chain orientation and Ramachandran congruity by use of the WhatIF program. The model shows the distribution of cysteines relevant for cross-linking. In addition, the arrow indicates the position 150 within the A domain, which was used for the site-directed introduction of a cysteine residue for FRET measurements.

Purification of the KdpFABC Complex. His_{14}-tagged KdpFABC complexes were purified via metal chelate affinity chromatography. Cells were lysed by passage through a cell fractionator (Basic Z cell disrupter, Constant Systems Ltd.) in 50 mM Tris-HCl at pH 7.5, 20 mM $MgCl_2$, 10% (v/v) glycerol, and 0.5 mM phenylmethylsulphonyl fluoride (PMSF). Cell debris was pelleted at 10000*g* for 15 min, and membranes were subsequently harvested by centrifugation at 160000*g* for 90 min. The membrane pellet was suspended in 50 mM Tris-HCl at pH 7.5, 10 mM $MgCl_2$, 10% (v/v) glycerol, 0.5 mM PMSF, and 1 mM dithiothreitol (DTT) at a protein concentration of 5 mg/mL, and membrane proteins were solubilized using 1% (v/v) aminoxide WS-35 (Goldschmidt) for 30 min on ice with gentle stirring. Solubilized proteins were separated by centrifugation at 100000*g* for 90 min, and the supernatant was applied to nickel−nitrilotriacetic acid (Ni−NTA) agarose (Qiagen) pre-equilibrated with 50 mM Tris/HCl at pH 7.5, 10 mM imidazole, 20 mM $MgCl_2$, 10% (v/v) glycerol, 150 mM NaCl, 0.5 mM PMSF, and 0.2% (v/v) aminoxide WS-35. After protein binding at 4 °C with gentle agitation for 60 min, the Ni−NTA slurry was transferred into a glass column and developed on an Äkta-FPLC (Amersham Biosciences) at a flow rate of 0.5 mL/min. The column was washed with the same buffer contain-

[1] Abbreviations: CuP, copper 1,10-phenanthroline; ECL, enhanced chemiluminescence; FRET, fluorescence resonance energy transfer; HRP, horseradish peroxidase; IgG, immune globulin G; MES, 2-(*N*-morpholino)ethanesulfonic acid; Ni−NTA, nickel−nitrilotriacetic acid; PMSF, phenylmethanesulfonylflouride; SDS−PAGE, sodium dodecyl sulfate−polyacrylamide gel electrophoresis; TEM, transmission electron microscopy; Tris, tris(hydroxymethyl)aminomethane.

ing 20 mM imidazole prior to the elution of KdpFABC with 130 mM imidazole. Corresponding fractions were concentrated by use of Amicon Ultra-4 Ultracell 30K centrifugal filter devices (Millipore) at 3000*g* and 4 °C for subsequent size-exclusion chromatography. Samples were loaded on a 10/30 Superdex-S200 column (Amersham Biosciences) equilibrated with 50 mM Tris-HCl at pH 7.5, 0.5 mM PMSF, and 0.2% (v/v) aminoxide WS-35 and developed at a flow rate of 0.5 mL/min. Protein-containing peak fractions were again pooled and concentrated as described above. In the case of subsequent electron microscopic analyses, the column was developed with 50 mM 2-(*N*-morpholino)ethanesulfonic acid (MES) at pH 6.5, 0.5 mM PMSF, and 0.2% (v/v) aminoxide WS-35.

Reconstitution of the KdpFABC Complex. Reconstitution of KdpFABC into proteoliposomes was carried out on the basis of established protocols (*21*). Preformed liposomes were prepared according to ref *22* with the following modifications. *E. coli* lipids (10 mg/mL chloroform solution, Avanti Polar Lipids) were evaporated under a gentle stream of argon and redissolved in a concentration of 5 mg/mL in detergent buffer. Preformed liposomes were finally dialyzed against 50 mM Tris-HCl at pH 7.0 and 2 mM β-mercaptoethanol and sized through 0.4 μm polycarbonate membranes (Whatman). Purified KdpFABC was mixed with preformed liposomes at a protein/lipid ratio of 1:20 in 50 mM Tris-HCl at pH 7.0. Liposomes were partially solubilized by the addition of 0.35% (v/v) of Triton X-100 (Merck). After 30 min, pretreated BioBeads SM-2 (Biorad) (*23*) were added in a detergent/BioBeads ratio of 1:10 followed by incubation for 90 min. This step was repeated with BioBeads added at a ratio of 1:20. Finally, BioBeads were added at a ratio of 1:40 followed by incubation overnight at 4 °C. Subsequently, the BioBeads were separated from the sample, and proteoliposomes were pelleted at 180000*g*, washed with 50 mM Tris-HCl at pH 7.25 to remove unincorporated protein, and subsequently resuspended in 50 mM Tris-HCl at pH 7.25 at a 6-fold concentration. Because of the interfering high amounts of lipids, the protein concentrations within proteoliposome samples were determined via comparative sodium dodecyl sulfate−polyacrylamide gel electrophoresis (SDS−PAGE) using 16.5% T/6% C separating gels together with 4% T/3% C stacking gels according to ref *24* with calibrated KdpFABC preparations and both silver and Coomassie staining.

ATPase Activity Assay. ATPase activities of purified KdpFABC complexes were determined using the microtiter plate assay of Henkel et al. (*25*) following the modifications described in ref *26*. A total of 0.5 μg of purified protein was routinely used for a single measurement. Protein concentrations in the absence of lipids were assayed with the bicinchoninic acid assay used as recommended by the supplier (Pierce) with bovine serum albumin as the standard.

Cross-link Studies. Cross-linking of purified KdpFABC complexes was performed by copper 1,10-phenanthroline treatment, which mediates the formation of disulfide bonds between neighboring cysteine residues. For cross-link formation, 5 μg of KdpFABC was incubated in 50 mM Tris-HCl at pH 7.5 and 0.2% (v/v) aminoxide WS-35 together with 1 mM copper 1,10-phenanthroline for 30 min at room temperature. One half of the sample was subsequently incubated with 10 mM β-mercaproethanol for 30 min at room temperature to reduce cross-links as a proof of specificity. Samples were then subjected to SDS−PAGE. For samples with reduced cross-links, the SDS−PAGE loading buffer contained 2% (v/v) β-mercaptoethanol. Quantification of relative cross-link yields was performed after densitometric scanning of gels by use of ImageQuaNT. The sum of all KdpB band intensities (i.e., cross-linked and non-cross-linked KdpB) in the cross-link sample served as the 100% reference, whereas a plain area of the gel was taken as the background density.

Western Blotting. Immunoblotting was performed as described by Deckers-Hebestreit and Altendorf (*28*) using the ECL Western blotting detection system (Pierce). For immunodecoration, a polyclonal rabbit anti-KdpB antiserum was used at a dilution of 1:10 000, together with a secondary mouse antirabbit IgG/HRP conjugate (Pierce) at the same dilution.

Analytical Size-Exclusion Chromatography. For the determination of the apparent molecular weight and the oligomeric state of KdpFABC, 100 μg of isolated KdpFABC complexes was cross-linked as described above. Subsequently, the sample containing both cross-linked and non-cross-linked fractions of the enzyme was loaded on a 10/30 Superdex-200 gel-filtration column, which was developed with 50 mM Tris-HCl at pH 7.5, 0.5 mM PMSF, and 0.2% (v/v) aminoxide WS-35 at a flow rate of 0.5 mL/min. Size calibration of the column was performed in the same buffer by use of the "high molecular weight gel filtration calibration kit" (Amersham Bioscience).

Electron Microscopy and Multireference Alignment. Purified KdpFABC complexes were diluted to a concentration of 2–10 μg/mL in 50 mM MES at pH 6.0, 50 mM NaCl, 5 mM $MgCl_2$, and 5 mM $CaCl_2$. A drop of the solution was then applied to freshly glow-discharged carbon-coated copper grids (400 mesh). After 1 min of incubation, the grid was washed 3 times with distilled water, followed by four washing steps with 2% (w/v) uranylacetic acid. After a short drying period, samples were examined in a CM-120 Biotwin (FEI Company) transmission electron microscope operated at 100 kV. Images were recorded at a nominal magnification of 46000× on Kodak S0163 films. Micrographs were scanned by use of a Zeiss Scai scanner using a step size of 14 μm for further analysis. Single-particle images were selected and boxed using the MRC software package according to ref *29*. Basic image processing was performed with the IMAGIC V package (*30*).

Fluorescence Labeling of Cysteines. All labeling reactions were carried out in the dark. To prevent the essential membrane-embedded native cysteines in KdpB from labeling, reconstituted KdpFABC complexes were used, in which these cysteines are shielded by the hydrophobic lipid environment. Proteoliposomes were diluted to a protein concentration of 3.2 μM in 50 mM Tris-HCl at pH 7.25 and 80 μM TCEP and labeled with 128 μM ATTO 655-maleimide (ATTO-TEC). After incubation for 2 h at room temperature, unbound label was completely removed by centrifugation (10 min, 200000*g*), followed by three additional washing steps in 50 mM Tris-HCl at pH 7.25. Subsequently, the labeling procedure was repeated with ATTO 488-maleimide the same way to create a mixed population of incorporated labels. Labeling efficiency was calculated using the KdpFABC concentration determined via SDS−PAGE as described above together with the fluoro-

phore absorption at 501 nm for ATTO 488 ($\epsilon = 90\,000\ M^{-1}\ cm^{-1}$) and at 663 nm for ATTO 655 ($\epsilon = 125\,000\ M^{-1}\ cm^{-1}$). To minimize light scattering effects, a corresponding aliquot of the labeled proteoliposome sample was solubilized with 2% (v/v) Triton-X-100. Finally, labeled proteoliposomes were diluted with preformed plain control liposomes without any protein to adjust a KdpFABC/liposome ratio of 0.2 or 5. Subsequently, solubilization with 1% (w/v) Triton-X-100 and consecutive detergent removal as described above allowed for an equal distribution of the reconstituted and labeled KdpFABC complexes. Proteoliposomes were stored at 4 °C and used for FRET measurements within 1 week.

FRET Analysis. Single-molecule fluorescence measurements of freely diffusing KdpFABC complexes in liposomes were performed at room temperature on a custom-designed confocal microscope (on the basis of an Olympus IX71 stage) similar to that described in ref *31*. Droplets (50 μL) of the labeled proteoliposomes with the given KdpFABC/liposome ratios of 0.2 and 5 were placed on a glass coverslip. For fluorescence excitation, the 488 nm laser line of an argon ion laser (Spectra Physics model 2020-03 S) was attenuated to 150 μW and focused into the aqueous solution by a water-immersion objective (UApo/340, 40×, N.A. 1.15; Olympus) generating a nearly diffraction-limited laser spot. Confocal detection volumes between 5 and 15 fl were obtained in combination with a 100 μm pinhole in the detection pathway to reject out-of-focus fluorescence. A dichroic mirror (c488-RDC; AHF) was used to suppress back-scattered laser light in epifluorescence configuration. Fluorescence from single molecules was detected by avalanche photodiodes (SPCM-AQR-14, Perkin-Elmer) after passing an interference filter (HQ 532/70 for ATTO 488 and HQ 665nm LP for ATTO 655; AHF, Germany). Photons were counted in two channels in parallel in the spectral range of 497–567 nm (ATTO 488) and above 665 nm (ATTO 655) by use of a PC card for time-correlated single-photon counting (SPC-630; Becker and Hickl) at 50 ns time resolution. Solutions of rhodamine 6 G or rhodamine 110 were used as references for the calibration of the confocal detection volume. Residual fluorescent impurities in the buffer solutions were removed by the addition of activated charcoal granula (Merck) and vigorous stirring for several hours. The average buffer background signal was around 3−6 photons/ms in both channels.

Proteoliposome samples were diluted in a way that only one liposome was present in the confocal volume at any time. Individual proteoliposomes with fluorescently labeled KdpFABC complexes traversing the detection volume were identified as clearly separated photon bursts in the fluorescence time trajectories. Intensity thresholds were applied to discriminate a photon burst from the background by use of the custom-made Burst Analyzer (*32*) software. The proximity factor *P*, which quantifies FRET acceptor intensity in relation to total intensity, was calculated in 1 ms time intervals for each photon burst. If the standard deviation of the proximity factor was less than 15% within the burst, the average proximity factor was calculated and added to the proximity factor histogram.

RESULTS

Cross-linking of KdpB Subunits. Cross-link studies were extensively used in the field of P-type ATPases to determine oligomeric states or subunit interactions, for example, in the case of the Na^+/K^+-ATPase (*33, 34*) and SERCA (*35*). In case of the KdpFABC complex, we used copper 1,10-phenanthroline (CuP), which oxidizes two adjacent cysteines to form a reducible disulfide bond. In addition to the formation of S−S bridges, CuP-induced cross-linking of cysteines is also reported to occur covalently to tyrosine, histidine, and tryptophane residues (*36*), which, in contrast to disulfide bonds, cannot be reduced and, thus, can clearly be discriminated. The KdpFABC complex comprises six cysteine residues within KdpA and six cysteines in the KdpB polypeptide, which leads to four possible types of cross-link products. First, intramolecular cross-linking in both KdpB and KdpA could appear as well as an intermolecular cross-link between KdpB and KdpA. The formation of these cross-link products is possible in both monomeric as well as oligomeric KdpFABC complexes. In contrast, the formation of intermolecular cross-links between two KdpB or KdpA subunits would clearly argue in favor of an oligomeric assembly of the KdpFABC complex.

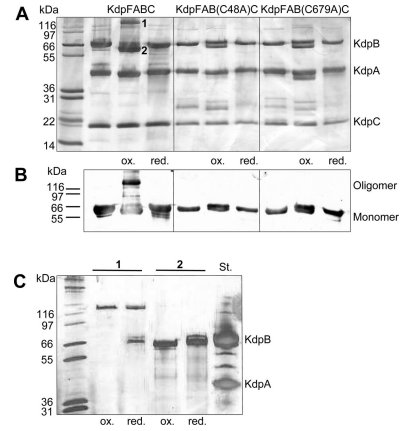

FIGURE 2: Cross-linking of isolated KdpFABC complexes with copper-phenanthroline. (A) Cross-linking of isolated KdpFABC complexes. A total of 5 μg of either wild-type or mutant KdpFABC complexes with single cysteine substitutions (C48A or C679A in KdpB as indicated) were separated by SDS−PAGE and stained with silver. "ox." complexes were cross-linked with 1 mM copper 1,10-phenanthroline for 30 min. "red." cross-links were subsequently reduced with 10 mM β-mercaptoethanol for 30 min. In either case of the cysteine substitutions, the intermolecular cross-link product was not visible. **1** and **2** depict the inter- and intramolecular cross-link products, respectively, taken for rechromatography in C. (B) Western blot analysis of A. KdpB was detected by the use of polyclonal anti-KdpB antibodies together with HRP-conjugated secondary antibodies and chemiluminescence detection. "Oligomer" refers to the intermolecular cross-link product of KdpB, whereas "monomer" refers to both the non-cross-linked KdpB population and the intramolecular KdpB cross-link product. (C) Analysis of the cross-link products **1** and **2** from A, demonstrating that only KdpB is present in the cross-link products. Bands **1** and **2** from A were excised and eluted from the gel in the absence ("ox.") or presence of 10 mM β-mercaptoethanol ("red."). Proteins were again separated via SDS−PAGE and detected by silver staining. "St." is the KdpFABC standard.

Incubation of isolated wild-type KdpFABC with CuP and subsequent SDS−PAGE revealed a 70% loss of the KdpB band as judged by densitometric scanning of the gel (Figure 2A, "ox."). Instead, a band with a lower apparent molecular weight of about 60 kDa was visible with a yield of 42% (band 2) together with a high-molecular-weight protein band of apparently 125–140 kDa (28%; band 1), both of which reacted with anti-KdpB antibodies (Figure 2B). Cross-link

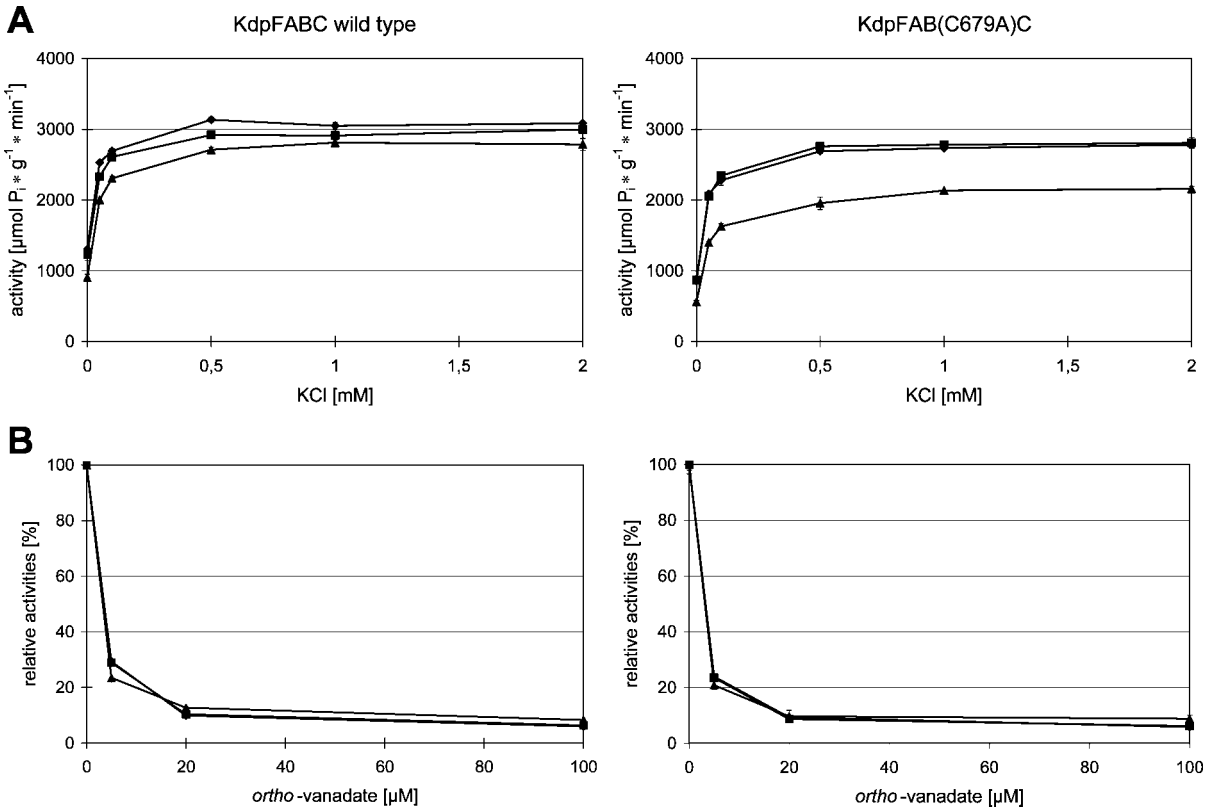

FIGURE 3: Effect of cross-linking on the catalytic properties of wild-type and mutant KdpFABC complexes. Isolated KdpFABC wild-type or KdpFAB(C679A)C mutant complexes, in which one of the cysteine residues responsible for cross-linking has been eliminated, were assayed in triplicate for K^+-stimulated ATPase activity (A) and *ortho*-vanadate inhibition (B). ◆, no addition of a cross-linker; ■, addition of 1 mM CuP; and ▲, subsequent addition of 10 mM β-mercaptoethanol.

formation was again completely reduced by the addition of mercaptoethanol ("red."). Rechromatography of both cross-link products by reducing SDS−PAGE led to the formation of only the 72 kDa KdpB band, although in the case of the higher molecular-weight cross-link product, the cross-link could not completely be reduced by the addition of β-mercaptoethanol (Figure 2C). However, because only the 72 kDa KdpB band was present as a result of the cross-link reversal, it can be assumed that the cross-link product exclusively contained KdpB. These results demonstrate that both cross-link products only contained the KdpB subunit. Whereas the 60 kDa cross-link product was indicative of an intramolecular cross-link within KdpB accelerating its mobility in SDS−PAGE, the higher molecular-weight cross-link product most likely represents a KdpB homodimer. The distribution of the six cysteines within the structural model of KdpB predicts only two pairs of cysteines to form intramolecular disulfide bridges (Figure 1). Cys-261 and Cys-609 in the center of the transmembrane segment are in S−S-bonding distance to each other as well as are Cys-142 and Cys-191, which are located in the actuator domain and represent the best candidates with respect to their accessibility toward the hydrophilic cross-linking agent. This view is supported by CuP-induced cross-linking with the isolated, soluble A domain of KdpB (*27*), which exhibited the same cross-link pattern (data not shown).

The best candidates for triggering the formation of a KdpB homodimer upon cross-linking are the relatively exposed, probably periplasmic residues Cys-48 and Cys-679 (Figure 1). Hence, both cysteines were exchanged separately to alanine. The resulting KdpFABC complexes exhibited almost the same K^+-stimulated and *ortho*-vanadate-inhibited ATPase activity as the wild type (see below) and were taken for corresponding cross-link analyses (parts A and B of Figure 2). Whereas the intramolecular cross-link product was again formed in both constructs as expected, the intermolecular cross-link product was clearly absent in both the KdpB-C48A and the KdpB-C679A construct, which demonstrates that both cysteine residues are involved in the formation of the intermolecular cross-link product by a direct S−S bridging.

Neither the inter- nor intramolecular cross-link had any significant inhibitory effect on the activity of the enzyme complex. Cross-linked KdpFABC in the presence of CuP behaved almost essentially as the non-cross-linked complex with respect to K^+-stimulated ATP hydrolysis and *ortho*-vanadate inhibition (Figure 3). The addition of CuP led to only a minimal drop in K^+-stimulated ATPase activity (Figure 3A), whereas vanadate inhibition was essentially the same (Figure 3B). To further elucidate the effect of cross-linking on the activity, the KdpB-C679A construct was also incorporated into this assay. Again, the complex in the absence of the cross-linking agent behaved essentially the same as in the case of the presence of CuP. Only the addition of β-mercaptoethanol (to again dissolve the cross-link) led to a drop in activity (but not in the efficiency of vanadate inhibition), which is rather due to an inhibitory effect of the reducing agent itself. The fact that the cross-linking of two KdpFABC complexes had hardly any effect on the activity of the enzyme demonstrates that, on the one hand, the cysteine bridging did not occur because of artificial and inhibitory configurations triggered by the cross-linking agent and, on the other hand, it shows that the KdpFABC complex

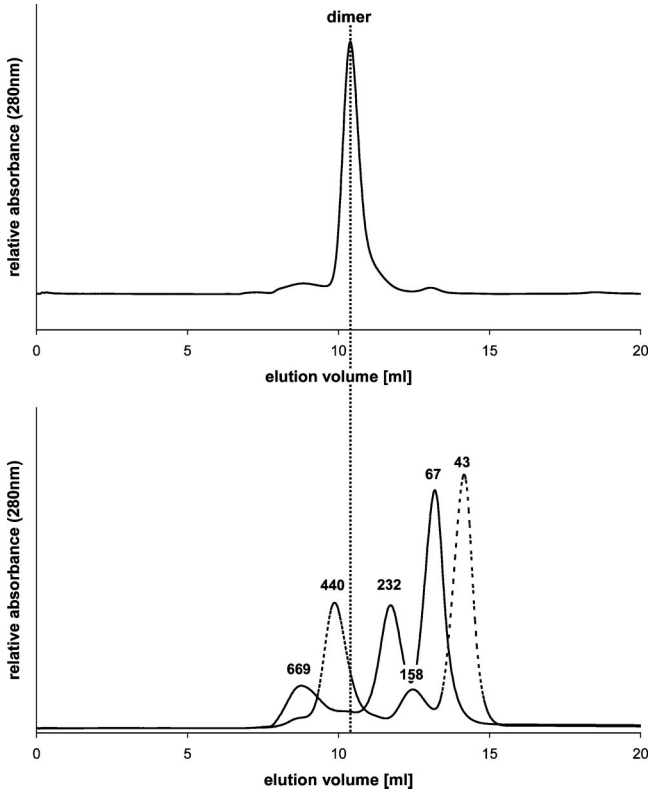

FIGURE 4: Size-exclusion chromatography of isolated and cross-linked KdpFABC complexes. A total of 100 μg of isolated KdpFABC complexes was cross-linked with 3 mM copper-1,10 phenanthroline for 30 min and analyzed by gel filtration (upper panel). The gel-filtration column was calibrated with standard proteins in the same buffer (lower panel; standard protein molecular weights in kilodaltons as indicated). The dotted line indicates the position of a dimeric KdpFABC with a calculated size of approximately 354.6 kDa.

already exists as a dimer, which is only non-invasively fixed by the cross-linking agent.

Size-Exclusion Chromatography. Although the cross-linking analyses provided first hints for the formation of a functional KdpFABC oligomer, the cross-link yield for the oligomer was only about one-third because of the use of native cysteines, which were not introduced specifically for achieving maximal cross-linking rates. To investigate whether this oligomer represents the native state of the isolated enzyme and, thus, constitutes a homodimer, a cross-linked KdpFABC preparation was analyzed by size-exclusion chromatography (Figure 4). If the cross-linked KdpFABC preparation contained a mixed population of monomers and artificially generated dimers by cross-linking, two distinct peaks should clearly be visible upon gel filtration even with a cross-link yield of only about 30%. The elution profile demonstrates that the cross-linked KdpFABC preparation containing two-thirds of non-cross-linked enzyme together with one-third of cross-linked complexes yielded only one single peak at a retention time, which was identical to the elution profile of the complex in the absence of the cross-linking agent. Hence, this single protein peak represents a homodimer, which does not alter its chromatographic properties upon cross-linking. Size calibration of the column by use of standard proteins in the same detergent buffer system revealed an apparent molecular mass of the eluted KdpFABC complex of about 350 kDa (dotted line), which is only 35 kDa larger than the calculated molecular mass of a KdpFABC homodimer. Because the enzyme complex represents a membrane-embedded protein with only little hydrophilic extensions, this 10% increase in molecular mass is most likely due to the presence of detergent molecules covering most of the surface of the protein. Thus, these results show that the isolated KdpFABC forms a homogeneous population of homodimers without the need of artificial cross-linking.

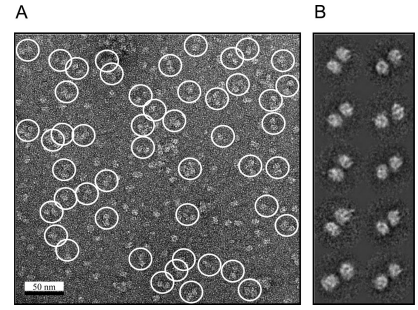

FIGURE 5: Electron microscopy of negatively stained KdpFABC complexes. (A) Isolated KdpFABC complexes were negatively stained with 2% (w/v) uranylacetic acid and analyzed by transmission electron microscopy. Dimeric particles are highlighted by circles. (B) Single-particle analysis of dimeric KdpFABC complexes. A total of 2500 single particles representing a dimeric configuration were selected from the scanned electron micrographs such as that presented in A and taken for analysis. Boxing of particles, image processing, alignment, and classification were performed as described (*29, 30*). The homogeneity of the KdpFABC homodimer is demonstrated by 10 representative class-sum averages, each of which comprising the averaged surface shape of particle subgroups with highly similar properties.

Electron Microscopy and Multireference Alignment. The experiments thus far revealed that the KdpFABC complex is purified in a dimeric form with neighboring KdpB subunits. To gain further information about the assembly of the dimer, purified KdpFABC complexes were negatively stained with uranylacetic acid and subjected to electron microscopic analyses (Figure 5). The corresponding micrographs revealed a monodisperse distribution of particles with a large fraction of dimeric complexes with a ratio of up to 50% with respect to the monomer (Figure 5A). In addition, the micrographs also revealed a large number of monomeric complexes, although the preparation contained a homogeneous population of homodimer as demonstrated above. The fraction of monomers is, thus, most likely due to the high dilution of the protein to obtain single particles in electron microscopy (20–50 nM), which triggers a dissociation of the homodimer. Higher oligomers were only found infrequently, and they did not exhibit a reproducible configuration, thus arguing in favor of the notion that only dimers represent the oligomeric state of KdpFABC. However, to judge whether the homodimer also represents a homogeneous structural assembly, 2500 dimeric complexes were selected from the data set for a multireference alignment and subsequent classification with respect to similarities in shape and size (Figure 5B). The resulting different class-sum averages comprising the averaged surface shape of particle subgroups with highly similar properties displayed an almost congruent shape with no deviating distortions or lacking subunits, thus demonstrating that the homodimer population is also homogeneous with respect to its structural assembly.

Single-Molecule FRET Analyses of Reconstituted KdpFABC. The results obtained thus far strongly argue in favor of the formation of a KdpFABC homodimer above concen-

trations of about 50 nM. Furthermore, our experiments thus far only aimed at the characterization of isolated KdpFABC complexes. Thus, in the final set of experiments, the oligomeric state of the KdpFABC complex was analyzed in proteoliposomes by single-molecule fluorescence detection.

In principle, femtoliter-sized observation volumes in confocal microscopy allow for counting and characterization of each fluorescently labeled KdpFABC complex traversing the laser spot one after another. Fluorescence of KdpFABC is recorded as individual photon bursts, which are separated in time. To discriminate monomers and dimers, a mixture of KdpFABC complexes labeled with either ATTO488-maleimide or ATTO655-maleimide was reconstituted into liposomes. ATTO655 fluorescence is not excited directly by the 488 nm laser. However, for dimeric complexes, the close proximity between two different fluorophores enables efficient fluorescence energy transfer from ATTO488 (FRET donor, bound on one complex) to ATTO655 (FRET acceptor) on the adjacent KdpFABC. The distance dependence of the FRET efficiency between donor and acceptor fluorophores is described by the Förster equation (*37*)

$$E_{\mathrm{FRET}} = \frac{R_0^6}{R_0^6 + r_{\mathrm{DA}}^6} \quad (1)$$

with R_0 representing the Förster radius (i.e., the fluorophore distance for 50% energy transfer) and r_{DA} representing the actual distance between the donor and acceptor. For the pair of dyes ATTO488 and ATTO655, the Förster radius is $R_0 = 5.0$ nm (given by the supplier). Accordingly, detecting ATTO655 fluorescence in a single proteoliposome clearly indicates a dimeric KdpFABC state. Hence, the formation of monomers or dimers of KdpFABC can be monitored by counting the number of proteoliposomes exhibiting FRET in relation to those showing no energy transfer.

For the site-specific incorporation of the FRET labels, all native cysteines were substituted by alanine or serine, depending upon the proposed hydrophobicity of the environment. Whereas the six cysteines of KdpA as well as four of the six cysteine residues in KdpB could be replaced without any effect on enzyme function, the membrane-embedded cysteines KdpB-C261 and KdpB-C679 turned out to be essential for enzyme activity and were, thus, not replaced in the labeling assay. However, because of their membrane-embedded location in the proteoliposomes, these two residues were prevented from labeling by the hydrophilic fluorescent maleimides. This was shown by SDS−PAGE analysis with subsequent staining and UV detection of the ATTO 488 label (Figure 6). With the labeling procedure chosen, plain liposomes showed no unspecific binding of the ATTO dye nor did they contain any contaminating proteins (lane 1). Although 12 cysteines are present in the wild-type KdpFABC complex, only slight traces of labeling were found in the case of the KdpB subunit, which are even hard to be seen on the corresponding gel upon UV illumination (lane 2). However, to definitely ensure specific labeling at a distinct position within a zero background, the cysteines were completely replaced as described above. Accordingly, no unspecific labeling could be observed with the cysteine-free complexes (lane 3). Also the reintroduced cysteines at position 261 and 679 in KdpB did not lead to detectable binding of the fluorescent probe (lanes 4–5), thereby ensuring

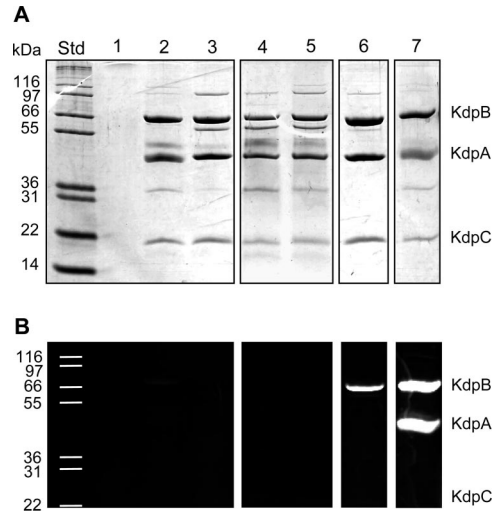

FIGURE 6: Protection of membrane-integrated cysteines in liposomes and specificity of labeling of the inserted cysteines. Isolated KdpFABC, KdpFABCΔCys (KdpFABC complexes, in which all cysteine residues have been replaced), and KdpFABCΔCys with different cysteine substitutions were reconstituted into liposomes at a protein/lipid ratio of 1:20 followed by labeling of 5 μg of protein with ATTO488-maleimide in a complex/dye ratio of 1:10. Subsequently, labeled proteoliposomes were subjected to SDS−PAGE. Proteins were either stained with Coomassie (A) or visualized by exposition on a UV transilluminator (B). Std, molecular-mass standard; 1, protein-free liposomes; 2, KdpFABC wild type; 3, KdpFABCΔCys; 4, KdpFABCΔCys-KdpB:A261C; 5, KdpFABCΔCys-KdpB:A261C/A609C; 6, KdpFABCΔCys-KdpB:G150C; and 7, KdpFABC wild type denatured with 1% (w/v) SDS prior to the addition of the fluorophore.

an absolutely background-free labeling of the target. For a selective labeling of only the A domain of KdpB, a cysteine residue was then introduced at an exposed position by use of a KdpB-G150C exchange (Figure 1), which resulted in the specific binding of the fluorescent probe upon reaction with the ATTO maleimide (lane 6). Labeling was carried out at a rather high protein/lipid ratio (1:20), which resulted in approximately 60 KdpFABC monomers per liposome, assuming a liposome diameter of 200 nm after sizing and a typical enzyme incorporation rate of 60%. The labeling had no influence on enzyme activity with respect to K^+-stimulated ATP hydrolysis and inhibition of ATPase by *ortho*-vanadate. The labeling ratio for the ATTO 655 acceptor maleimide was calculated to be 47%, and for the ATTO 488 donor maleimide, only 6% were achieved. Labeling ratios frequently found in single-molecule FRET analysis of proteoliposomes with highly diluted protein are around 10%. Higher concentrations of fluorophores to achieve an accordingly higher labeling efficiency result in unspecific labeling of the lipid component because of the low protein concentration as well as in the labeling of membrane-embedded cysteines. In addition, the two ATTO dyes comprise a different basic chemical structure, which is not published by the supplier, which accounts for a different behavior in the labeling process. The labeling ratios were, thus, chosen with respect to a minimal lipid labeling with concomitant specific binding to only the inserted cysteine in the A domain. Although the labeling ratio in the case of ATTO 488 is just 6%, the labeling is assumed to occur without a preference for a possible subpopulation of particles, because the preparation has previously been shown to be homogeneous and no ligand was present, which could trigger different

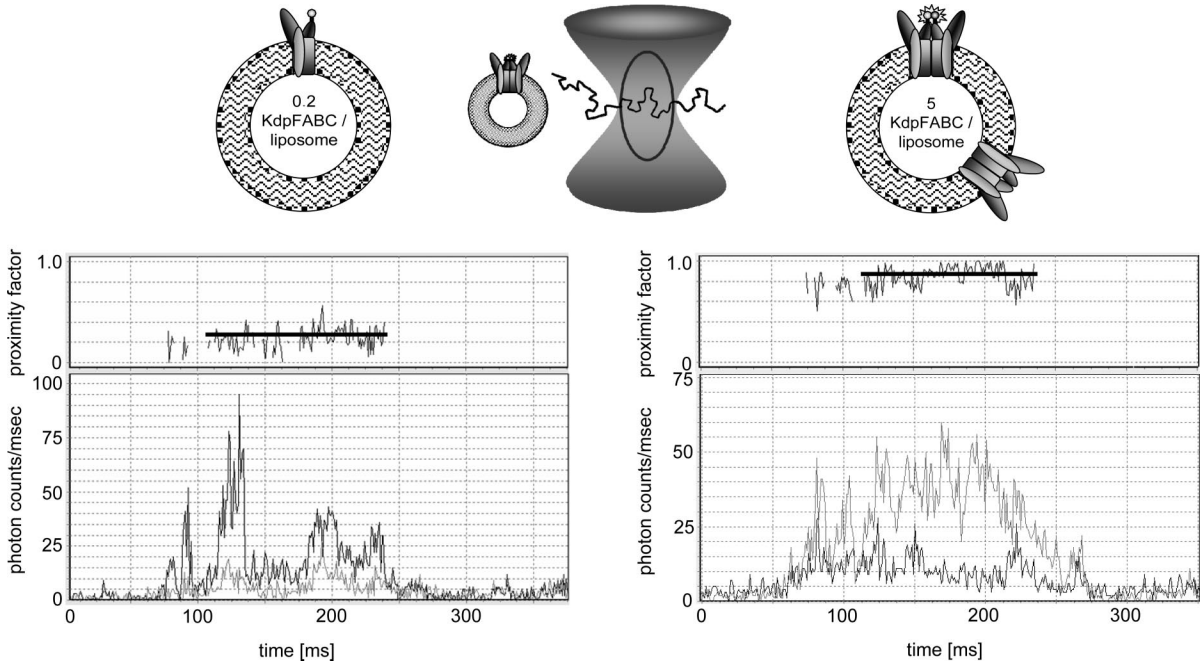

FIGURE 7: Single-molecule FRET analysis of reconstituted KdpFABC complexes. Isolated KdpFABC was reconstituted into liposomes at calculated complex/liposome ratios of 0.2 (left) and 5 (right). KdpFABC complexes were heterogeneously labeled at a specific cysteine residue introduced into the A domain with both donor and acceptor. During the measurements, only one liposome was present in the confocal volume at any time, resulting in fluorescence intensity trajectories upon excitation of the donor dye (lower panel). The trajectories of a representative data set are shown together with the corresponding calculated proximity factor representing the FRET efficiency.

conformations. In addition, as already mentioned, the low labeling ratio is a consequence of the prevention of unspecific binding of the probe.

The differently labeled KdpFABC complexes were mixed and co-reconstituted into liposomes, resulting in proteoliposomes containing only one complex with either ATTO488 or ATTO655 or oligomeric complexes. The monomer/liposome ratio was adjusted to 0.2 and 5 with plain control liposomes in the presence of detergent as described. The two concentrations chosen rather closely framed the apparent dissociation constant obtained from the electron microscopic analysis, whereas the calculated 0.2 complexes/liposome ratio ensured the presence of a maximal one enzyme complex per liposome at any time. Because the laser beam selectively excited ATTO488 as the donor molecule, only protein complexes with one or more donor molecules were detected by high fluorescence intensities in the FRET donor detection channel. Alternatively, complexes with one donor together with one acceptor fluorophore were identified by FRET, showing fluorescence in both the donor and acceptor channel simultaneously.

Labeled proteoliposomes were diluted until well-separated photon bursts with count rates of up to 150 photons/ms (typical of a freely diffusing single donor dye) could be observed in the confocal volume. In the lower trace panel of Figure 7, one representative photon burst for each monomer/liposome ratio is presented. In both time traces, fluorescence intensity increases and again decreases to the background level when a liposome enters and again leaves the detection volume, respectively. Overall, rather large fluctuations in the burst rates could be observed because the excitation power and, thus, the detected fluorescence depend upon the relative position of the fluorophore within the detection volume. Brownian motion caused these large fluctuations but without affecting the donor/acceptor fluorescence ratio.

For a KdpFABC/liposome ratio of 0.2, there were solely donor-only fluorescence bursts with no significant signals in the acceptor channel. However, at a reconstitution ratio of 5 KdpFABC/liposome there were obvious and distinct FRET events with strong fluorescence in the acceptor channel. This was further straightened out by calculating the mean proximity factor P per photon burst (as a measure of FRET efficiency) defined as the ratio of the background-corrected acceptor fluorescence intensity (I_A) divided by the sum of donor and acceptor intensities ($I_D + I_A$) (*38*)

$$P = I_A/(I_D + I_A) \quad (2)$$

The corresponding proximity factor time trajectory is plotted in the upper trace panel of Figure 7. In the case of 0.2 complexes/liposome, the mean proximity factor was rather low, well in accordance with the correspondingly low acceptor fluorescence signal. In strong contrast, the proximity factor increased to a value of 0.9 (reflecting 90% transfer efficiency by FRET), thereby clearly demonstrating a close vicinity of two neighboring ATTO488 and ATTO655 dyes and, thus, dimer formation.

For statistical evaluation, the normalized number of FRET events was plotted against the average proximity factor calculated for every selected burst (Figure 8A). The histogram clearly demonstrates that in the case of a 0.2 mixed-labeled complex/liposome ratio, the corresponding maximal proximity factor is almost congruent with that for the control (only labeled with the donor dye). This indicates a rather long distance (>10 nm) between two monomeric complexes within a single liposome. In contrast, the same mixed KdpFABC sample reconstituted at a 5 monomers/liposome ratio showed a significant shift toward high proximity factors

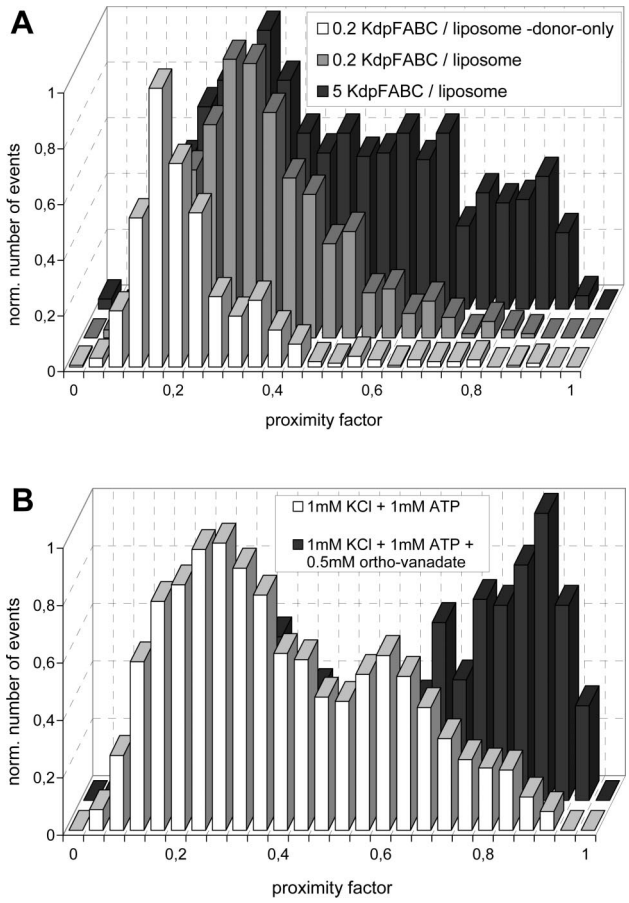

FIGURE 8: Histogram of proximity factors summarizing the single-molecule FRET analysis of reconstituted KdpFABC. (A) Isolated KdpFABC was reconstituted into liposomes at calculated complex/liposome ratios of 0.2 (light gray) and 5 (dark gray) and heterogeneously labeled with both donor and acceptor. White bars: distribution of proximity factors for the donor-labeled complex (donor-only control). Normalized distributions were calculated from 1 ms time intervals in 10 long-lasting photon bursts for each FRET efficiency state. High proximity factors (*P* values) indicate adjacent A domains within a KdpFABC dimer. (B) Influence of ligands on the distance between A domains of adjacent KdpB subunits. Isolated KdpFABC was reconstituted into liposomes at a calculated complex/liposome ratio of 5 and heterogeneously labeled with both donor and acceptor as in A. Single-molecule FRET analysis was performed in the presence of 1 mM KCl together with 1 mM ATP (white bars; catalysis conditions) as well as upon the subsequent addition of 0.5 mM *ortho*-vanadate (gray bars; E2-inhibited state).

(*P* > 0.5), representing FRET in adjacent KdpFABC complexes. As a control, Atto488-only labeled KdpFABC reconstituted at both 0.2 and 5 complexes/liposome exhibited a proximity factor maximum around 0.16. This *P* value was caused by spectral cross-talk; i.e., a small amount of the red-shifted ATTO488 fluorescence was detected in the acceptor channel. These findings are consistent with monomeric KdpFABC complexes at low concentrations of 0.2 complexes per liposome, whereas at higher concentrations (5 complexes per liposome) a KdpFABC dimer forms, which leads to FRET via adjacent A domains.

In a further attempt, the catalytic properties of the dimeric complex were probed with FRET analysis. Therefore, KdpFABC complexes were reconstituted at 5 complexes/liposome and analyzed in the presence of KCl and ATP (catalysis conditions) as well as in the presence of *otho*-vanadate (inhibition in the E2 state of the enzyme) (Figure 8B). Under conditions of catalysis, the *P* factor again displayed a rather broad distribution as in Figure 8A but with two distinct maxima located around 0.3 and 0.6, respectively. These two predominant distances between the A domains within the dimer could indicate rate-limiting steps during catalysis, although the maximum around 0.3 overlaps with the donor-only fluorescence. However, in the presence of the E2 inhibitor *ortho*-vanadate, the maximum of the proximity factor around 0.6 is significantly shifted toward high values peaking at 0.9, together with a decrease in the 0.3 *P* value maximum, which demonstrates that the complex is now trapped in another configuration (namely, E2), in which the A domains are close to each other.

DISCUSSION

P-type ATPases usually consist of only one single subunit, which mediates both ATP hydrolysis and ion transport. Some representatives exhibit additional regulatory subunits, such as phospholamban and calmodulin in the case of the Ca^{2+}-ATPase (SERCA) or the γ subunit of the Na^+/K^+-ATPase. Although much is known about the structure of this superfamily of enzymes, the oligomeric state of many P-type ATPases is only poorly understood. In the case of the *N. crassa* H^+-ATPase, the monomeric enzyme molecule is reported to translocate protons (*39*) but, with slight modifications in the purification protocol, large-scale preparations resulted in an active hexamer (*13, 14*). The oligomeric status of the Na^+/K^+-ATPase is also still a point of discussion. According to detailed studies on isoforms from canine and pig kidney, including ligand-binding and phosphorylation experiments as well as FRET and electron microscopy, a tetraprotomeric form $(\alpha\beta)_4$ is favored (*15, 40*). In this case, the α subunit represents the catalytic P-type ATPase subunit, with the highly glycosylated β subunit most likely playing a role in maturation and regulation of the complex. However, also monomeric isoforms of this enzyme were found in microsomes derived from duck salt glands (*41*). As the Na^+/K^+-ATPase, the gastric H^+/K^+-ATPase also consists of an α and a β subunit. The current data, which are mainly derived from cross-linking analysis, support the notion that the minimum structural unit is also a $(\alpha\beta)_2$ diprotomer (*42*).

In this work, we demonstrate by means of cross-linking experiments and gel filtration that the isolated KdpFABC complex from *E. coli* adopts a dimeric state after purification. Furthermore, as shown by electron microscopy and, more precisely in its native environment, by single-molecule FRET measurements, homodimer formation of isolated KdpFABC was only found at concentrations above 30–50 nM, whereas below these concentrations, the KdpFABC complex occurred as a monomer. These findings clearly demonstrate that dimer formation is dependent upon the concentration of the complex and favor a defined monomer/dimer equilibrium.

On the basis of the cross-linking experiments, a close vicinity of two KdpB subunits within a $Kdp(FABC)_2$ homodimer is clearly shown. Although both cysteine residues responsible for cross-link formation can be located in the SERCA-derived homology model of KdpB, the model does not allow for conclusions about the spatial arrangements of the neighboring KdpB subunits within the dimer for the following reason: Whereas Cys-48 is clearly located at a position facing the periplasm, the model provides no clear

information about the position of Cys-679, which is located next to the C terminus of KdpB. Because of the inherent flexibility of this stretch of residues in the model, it could be located both toward the periplasm or in the membrane. Furthermore, it could also be oriented to the front- or backside of the subunit. However, on the basis of the close proximity of Cys-48 and Cys-679 allowing disulfide bonding together with the notion that the flexible N and A domains have enough space for their movements within the reaction cycle, the most likely assembly is a face-to-face orientation of the two KdpB subunits. In such an orientation, the dimer interface would run through the transmembrane domain near the Rossman fold of the P domain. Interestingly, this assumption is in accordance with data obtained from the overexpression of the soluble large cytoplasmic domain (LCD) of several P-type ATPases. The LCD includes both the N and P domains. For the Na^+/K^+-ATPase, the region responsible for the interaction of two α subunits within a LCD dimer was narrowed down to a stretch of 150 amino acids located within the C-terminal portion of the LCD, which is the P domain (*43*). Isolated LCD from SERCA expressed in *E. coli* as a fusion protein also tends to form dimers. Proteinase treatment of dimeric LCD resulted in the formation of the monomeric N domain, thus clearly pointing out that the self-association of the dimeric SERCA LCD also depends upon the P domain (*44*). The same observations were made with the LCD of the *Saccharomyces cerevisiae* plasma membrane H^+-ATPase. Whereas the entire LCD existed in a monomer/dimer equilibrium, a truncated LCD lacking the C terminus of the P domain formed only monomers (*45*). All of these data also suggest that the P domain is certainly involved in oligomer formation.

Whereas the cross-link analysis only points toward the formation of KdpFABC oligomers, the calibrated size-exclusion chromatography together with the electron microscopic data clearly revealed a homogeneous population of KdpFABC homodimers, which is subject to dissociation into its monomers upon dilution. The relative high amount of monomeric complexes is more a result of the high dilution of the complexes rather than the acid-staining procedure, because uranyl acetate is well-known to function as a very effective fixative, stabilizing proteins, lipids, and nucleic acids in a very rapid time scale of about 10 ms (*46–48*).

The single-molecule FRET measurements revealed that KdpFABC also forms dimers in its native environment. The mixture of KdpFABC complexes labeled with either donor or acceptor fluorophore and diluted to 5 KdpFABC per liposome showed a strong shift toward high FRET efficiency values, which clearly demonstrates a close vicinity of the donor and acceptor within a homodimer. In a liposome with a diameter of 200 nm, such vicinity is absolutely unlikely for freely diffusing monomers. Interestingly, the distribution of proximity factors in the case of 5 KdpFABC/liposome could be separated into three maxima instead of only two as expected (corresponding to only monomers and dimers each in a single configuration). Whereas the first proximity factor is located at 0.32 and represents the donor-only fraction of the dimeric KdpFABC, the high *P* value fraction splits into two populations, with maxima located between 0.52 and 0.68 and between 0.76 and 0.92, respectively. These two FRET populations likely represent two different orientations in the homodimer or two conformational states, for example, fluctuation between the E1 and the E2 state, which, of course, could not be observed in the case of monomeric KdpFABC at 0.2 complexes/liposome because of the lack of the FRET partner. This is further supported by our findings that the addition of *ortho*-vanadate to KdpFABC reconstituted at 5 complexes/liposome resulted in a distinct shift of the *P* values from a rather broad distribution with maxima around 0.3 and 0.6, which are indicative of a fluctuating distance between the fluorescent probes, toward a distinct maximum around 0.9, thereby pointing toward a fixed E2 conformation, in which the A domains are close to each other within the functional dimer. These findings already demonstrate the potential value of this technique beyond the mere study of dimer formation.

The discrimination between KdpFABC monomers and dimers in the FRET analysis indicates that the dissociation constant of the dimer is between the two concentrations used in the reconstitution. The exact determination of the dissociation constant by this FRET method is very complicated, because the concentration of the reconstituted complexes is too low to allow for a precise determination. However, these findings are in accordance with the observations made by electron microscopy. In this experiment, the concentration of KdpFABC complexes was around 20–50 nM with a monomer/dimer ratio of about 50%. In summary, a dissociation constant of the monomer/dimer equilibrium of 30−50 nM could be derived from our data, which is somewhat lower than dissociation constants reported from other P-type ATPases. The monomer/dimer equilibrium of the plasma membrane Ca^{2+}-ATPase, for example, has been determined at 140 ± 50 nM (*49*). In this context, it has to be noted that the KdpFABC complex comprises additional subunits, which are most likely also involved in dimer formation/interaction and, thus, could easily increase the binding affinity.

However, a dissociation constant in the nanomolar range strongly suggests a physiological relevance of homodimer formation. Recent single-molecule FRET analyses in our group revealed that also the monomeric form of KdpFABC is active (to be published). Therefore, the dimerization does not seem to be essential *in vivo* but most likely optimizes the catalytical properties of the enzyme. It is tempting to speculate about a possible cooperativity in catalysis. As mentioned above, oligomerization is found throughout the family of P-type ATPases, although its functional significance is not yet understood. Functional relevance of oligomerization has, thus, to be closely related to the common catalytic mechanism. Because the KdpFABC complex drastically differs from all other P-type ATPases with respect to the mode of ion translocation by a separate subunit, a common functional benefit of oligomerization is most likely restricted to the nucleotide binding/hydrolysis mechanism, and, thus, to the N, A, and P domains. Interestingly, as mentioned above, especially the P domain is reported to be involved in dimer formation, which could suggest a cooperative nucleotide interaction of P domains within the dimer. In KdpFABC, the situation is further complicated by the KdpC subunit, which was also shown to interact with the nucleotide (*12*). However, the function of KdpC is more in the direction of closing the nucleotide-binding pocket upon ATP binding rather than being involved in (de)phosphorylation of the conserved aspartate (*12*). In either case, the interaction with KdpC would be around the nucleotide-binding site and, thus,

on the opposing side of putatively interacting P domains. Most recently, the three-dimensional structure of the hydrophilic portion of the KdpFABC complex, except KdpC, was determined at low resolution with electron tomography of two-dimensional KdpFABC crystals (*50*). In these studies, the unit cell of the crystals contained a KdpFABC dimer, which appeared to be mediated by a contact between the N domains of KdpB, although the authors themselves stated that one can not be certain about the functional relevance of the crystallographic dimer seen in their maps. Nevertheless, the clarification of the physiological role of dimer formation turns out to be an interesting subject for further analysis.

ACKNOWLEDGMENT

Henrik Strahl is kindly acknowledged for the homology modeling of KdpB. We thank Nawid Zarrabi (University of Stuttgart) for providing the software "Burst Analyzer" used for the single-molecule FRET data analysis.

REFERENCES

1. Møller, J. V., Juul, B., and le Maire, M. (1996) Structural organization, ion transport, and energy transduction of P-type ATPases. *Biochim. Biophys. Acta 1286*, 1–51.
2. Toyoshima, C., Nakasako, M., Nomura, H., and Ogawa, H. (2000) Crystal structure of the calcium pump of sarcoplasmic reticulum at 2.6 Å resolution. *Nature 405*, 647–655.
3. Toyoshima, C., and Nomura, H. (2002) Structural changes in the calcium pump accompanying the dissociation of calcium. *Nature 418*, 605–611.
4. Toyoshima, C., Nomura, H., and Sugita, Y. (2003) Crystal structures of Ca^{2+}-ATPase in various physiological states. *Ann. N.Y. Acad. Sci. 986*, 1–8.
5. Toyoshima, C., and Mizutani, T. (2004) Crystal structure of the calcium pump with a bound ATP analogue. *Nature 430*, 529–535.
6. Olesen, C., Sørensen, T. L., Nielsen, R. C., Møller, J. V., and Nissen, P. (2004) Dephosphorylation of the calcium pump coupled to counterion occlusion. *Science 306*, 2251–2255.
7. Van der Laan, M., Gassel, M., and Altendorf, K. (2002) Characterization of amino acid substitutions in KdpA, the K^+-binding and -translocating subunit of the KdpFABC complex of *Escherichia coli*. *J. Bacteriol. 184*, 5491–5494.
8. Durell, S. R., Bakker, E. P., and Guy, H. R. (2000) Does the KdpA subunit from the high affinity K^+-translocating P-type KDPATPase have a structure similar to that of K^+ channels? *Biophys. J. 77*, 775–788.
9. Bramkamp, M., and Altendorf, K. (2005) Single amino acid substitution in the putative transmembrane helix V in KdpB of the KdpFABC complex of *Escherichia coli* uncouples ATPase activity and ion transport. *Biochemistry 44*, 8260–8266.
10. Gassel, M., Möllenkamp, T., Puppe, W., and Altendorf, K. (1999) The KdpF subunit is part of the K^+-translocating Kdp complex of *Escherichia coli* and is responsible for stabilization of the complex *in vitro*. *J. Biol. Chem. 274*, 37901–37907.
11. Gassel, M., and Altendorf, K. (2001) Analysis of KdpC of the K^+-transporting KdpFABC complex of *Escherichia coli*. *Eur. J. Biochem. 268*, 1772–1781.
12. Ahnert, F., Schmid, R., Altendorf, K., and Greie, J.-C. (2006) ATP binding properties of the soluble part of the KdpC subunit from the *Escherichia coli* K^+-transporting KdpFABC P-type ATPase. *Biochemistry 45*, 11038–11046.
13. Chadwick, C. C., Goormaghtigh, E., and Scarborough, G. A. (1987) A hexameric form of the *Neurospora crassa* plasma membrane H^+-ATPase. *Arch. Biochem. Biophys. 252*, 348–356.
14. Rhee, K.-H., Scarborough, G. A., and Henderson, R. (2002) Domain movements of plasma membrane H^+-ATPase: 3D structures of two states by electron cryo-microscopy. *EMBO J. 21*, 3582–3589.
15. Taniguchi, K., Kaya, S., Abe, K., and Mardh, S. (2001) The oligomeric nature of Na^+/K^+-transport ATPase. *J. Biochem. 129*, 335–342.
16. Chamberlain, B. K., Berenski, C. J., Jung, C. Y., and Fleischer, S. (1983) Determination of the oligomeric structure of the Ca^{2+} pump protein in canine cardiac sarcoplasmic reticulum membranes using radiation inactivation analysis. *J. Biol. Chem. 258*, 11997–12001.
17. Hymel, L., Maurer, A., Berenski, C., Jung, C. Y., and Fleischer, S. (1984) Target size of calcium pump protein from skeletal muscle sarcoplasmic reticulum. *J. Biol. Chem. 259*, 4890–4895.
18. Squier, T. C., Hughes, S. E., and Thomas, D. D. (1988) Rotational dynamics and protein−protein interactions in the Ca^{2+}-ATPase mechanism. *J. Biol. Chem. 263*, 9162–9170.
19. Chen, L., Yao, Q., Brungardt, K., Squier, T. C., and Bigelow, D. J. (1998) Changes in spatial arrangement between individual Ca^{2+}-ATPase polypeptide chains in response to phospholamban phosphorylation. *Ann. N.Y. Acad. Sci. 853*, 264–266.
20. Siebers, A., and Altendorf, K. (1988) The K^+-translocating Kdp-ATPase from *Escherichia coli*. Purification, enzymatic properties and production of complex- and subunit-specific antisera. *Eur. J. Biochem. 178*, 131–140.
21. Fendler, K., Dröse, S., Altendorf, K., and Bamberg, E. (1996) Electrogenic K^+ transport by the Kdp-ATPase of *Escherichia coli*. *Biochemistry 35*, 8009–8017.
22. Stalz, W. P., Greie, J.-C., Deckers-Hebestreit, G., and Altendorf, K. (2003) Direct interaction of subunits *a* and *b* of the F_O complex of *Escherichia coli* ATP synthase by forming an ab_2 subcomplex. *J. Biol. Chem. 278*, 27068–27071.
23. Holloway, P. W. (1973) A simple procedure for removal of Triton X-100 from protein samples. *Anal. Biochem. 53*, 304–308.
24. Schägger, H., and von Jagow, G. (1987) Tricin−sodium dodecyl sulfate−polyacrylamide gel electrophoresis for the separation of proteins in the range of 1 to 100 kDa. *Anal. Biochem. 166*, 368–379.
25. Henkel, R. D., van de Berg, J. L., and Walsh, R. A. (1988) A microassay for ATPase. *Anal. Biochem. 169*, 312–318.
26. Altendorf, K., Gassel, M., Puppe, W., Möllenkamp, T., Zeeck, A., Boddien, C., Fendler, K., Bamberg, E., and Dröse, S. (1998) Structure and function of the Kdp-ATPase of *Escherichia coli*. *Acta Physiol. Scand. 163*, 137–146.
27. Bramkamp, M. (2003) Characterization of the KdpFABC complex from *Escherichia coli*, of soluble subdomains from KdpB, and of a homologous protein of *Methanococcus jannaschii*, Ph.D. Thesis, University of Osnabrueck, Osnabrueck, Germany.
28. Deckers-Hebestreit, G., and Altendorf, K. (1986) Accessibility of F_O subunits from *Escherichia coli* ATP synthase. A study with subunit specific antisera. *Eur. J. Biochem. 161*, 225–231.
29. Crowther, R. A., Henderson, R., and Smith, J. M. (1996) MRC image processing programs. *J. Struct. Biol. 116*, 9–16.
30. Van Heel, M., Harauz, G., Orlova, E. V., Schmidt, R., and Schatz, M. (1996) A new generation of the IMAGIC image processing system. *J. Struct. Biol. 116*, 17–24.
31. Armbrüster, A., Hohn, C., Hermesdorf, A., Schumacher, K., Börsch, M., and Grüber, G. (2005) Evidence for major structural changes in subunit C of the vacuolar ATPase due to nucleotide binding. *FEBS Lett. 579*, 1961–1967.
32. Zimmermann, B., Diez, M., Zarrabi, N., Gräber, P., and Börsch, M. (2005) Movements of the ϵ-subunit during catalysis and activation in single membrane-bound H^+-ATP synthase. *EMBO J. 24*, 2053–2063.
33. Askari, A., and Huang, W. (1980) Na^+,K^+-ATPase: Half-of-the-subunits cross-linking reactivity suggests an oligomeric structure containing a minimum of four catalytic subunits. *Biochem. Biophys. Res. Commun. 93*, 448–453.
34. Karlish, S. J. D. (1997) Organization of the membrane domain of the Na^+/K^+-pump. *Ann. N.Y. Acad. Sci. 834*, 30–44.
35. Chen, Z., Stokes, D. L., Rice, W. J., and Jones, L. R. (2003) Spatial and dynamic interactions between phospholamban and the canine cardiac Ca^{2+} pump revealed with use of heterobifunctional cross-linking agents. *J. Biol. Chem. 278*, 48348–48356.
36. Watts, B. P., Barnard, M. L., and Turrens, J. F. (1995) Peroxynitrite-dependent chemiluminescence of aminoacids, proteins and intact cells. *Arch. Biochem. Biophys. 317*, 324–330.
37. Förster, T. (1948) Zwischenmolekulare energiewanderung und fluoreszenz. *Ann. Phys. 2*, 55–70.
38. Ha, T. (2001) Single-molecule fluorescence resonance energy transfer. *Methods 25*, 78–86.
39. Goormaghtigh, E., Chadwick, C., and Scarborough, G. A. (1986) Monomers of the *Neurospora* plasma membrane H^+-ATPase catalyze efficient proton translocation. *J. Biol. Chem. 261*, 7466–7471.
40. Ivanov, A. V., Modyanov, N. N., and Askari, A. (2002) Role of the self-association of β subunits in the oligomeric structure of Na^+,K^+-ATPase. *Biochem. J. 364*, 293–299.

41. Martin, D. W., Marecek, J., Scarlata, S., and Sachs, J. R. (2000) $\alpha\beta$ protomers of Na^+,K^+-ATPase from microsomes of duck salt gland are mostly monomeric: Formation of higher oligomers does not modify molecular activity. *Proc. Natl. Acad. Sci. U.S.A. 97*, 3195–3200.
42. Shin, J. M., and Sachs, G. (1996) Dimerization of the gastric H^+,K^+-ATPase. *J. Biol. Chem. 271*, 1904–1908.
43. Koster, J. C., Blanco, G., and Mercer, R. W. (1995) A cytoplasmic region of the Na^+,K^+-ATPase α-subunit is necessary for specific α/α association. *J. Biol. Chem. 270*, 14332–14339.
44. Carvalho-Alves, P. C., Hering, V. R., Oliveira, J. M. S., Salinas, R. K., and Verjovski-Almeida, S. (2000) Requirement of the hinge domain for dimerization of Ca^{2+}-ATPase large cytoplasmic portion expressed in bacteria. *Biochim. Biophys. Acta 1467*, 73–84.
45. Almeida, W. I., Martins, O. B., and Carvalho-Alves, P. C. (2006) Self-association of isolated large cytoplasmic domain of plasma membrane H^+-ATPase from *Saccharomyces cerevisiae*: Role of the phosphorylation domain in a general dimeric model for P-ATPases. *Biochim. Biophys. Acta 1758*, 1768–1776.
46. Glauert, A. M., and Lewis, P. R. (1998) Biological specimen preparation for transmission electron microscopy, in *Practical Methods in Electron Microscopy* (Glauert, A. M., Ed.) Vol. 17, Portland Press, London, U.K.
47. Hayat, M. A. (2000) Principles and techniques of electron microscopy, *Biological Applications*, 4th ed., Cambridge University Press, Cambridge, U.K.
48. Zhao, F. Q., and Craig, R. (2002) Capturing time-resolved changes in molecular structure by negative staining. *J. Struct. Biol. 141*, 43–52.
49. Levi, V., Rossi, J. P. F. C., Castello, P. R., and Flecha, L. G. (2002) Structural significance of the plasma membrane calcium pump oligomerization. *Biophys. J. 82*, 437–446.
50. Hu, G.-B., Rice, W. J., Dröse, S., Altendorf, K., and Stokes, D. L. (2007) Three-dimensional structure of the KdpFABC complex of *Escherichia coli* by electron tomography of two-dimensional crystals, *J. Struct. Biol.*, in press.

BI702038E